Buildup and Consumption of Species in Emulsion Droplets during Aqueous Suzuki Coupling Correlate with Yield

Hannah Peacock and Suzanne A. Blum*

Department of Chemistry, University of California, Irvine, Irvine, California 92697-2025, United States

ABSTRACT: Fluorescence lifetime imaging microscopy (FLIM) provides spatiotemporal resolution of the changing composition of emulsion droplets during an aqueous–surfactant Suzuki coupling. In contrast to previous investigations, the present experiments characterize the full course of a catalytic chemical reaction, addressing key questions about if and where reaction species build up, and correlating these microscale behaviors with bench-scale product yields. At low concentrations of (active) catalyst, droplet environments are stable; however, at higher concentrations, emulsion droplet environments change markedly, as indicated by the rise and fall of fluorescence lifetimes. These changes are consistent with buildup and consumption of reaction species inside the droplets. A combination of FLIM and brightfield imaging pinpoint limitations in catalyst solubility as controlling the rate and degree of buildup of species in droplets. These solubility limitations are also identified as the cause of a reaction induction period, and an origin of the rate-and-reproducibility advantage obtained by adding a THF as a cosolvent. The subsequent mechanistic model from these data led to a bench-scale reaction optimization, wherein premixing the catalyst components bypasses the catalyst induction period, resulting in a faster reaction at otherwise constant catalyst loading. The understanding generated by FLIM thus provides an early example of how understanding changes in droplet compositions on the microscale during ongoing aqueous–organic reactions can be leveraged for enhancing efficiencies in bench-scale reactions.

Introduction

Organic chemistry in water provides a promising sustainable alternative to reactions in organic solvents. Addition of surfactants can optimize these reactions by solubilizing organics and/or stabilizing micelles and emulsion droplets. Notable applications of surfactant-based reactions, including palladium-catalyzed cross-coupling, have been developed in agrochemical and pharmaceutical[1–6] and academic[7–9] settings. The mechanistic underpinnings of these complicated reactions are poorly understood, however, limiting broader implementation of this promising technology. For example, under the high-substrate concentrations germane to bench-scale synthetic reactions, phase separation occurs,[10,11] leading to multiple possible locations for substrates and intermediates–and thus for reactions to occur (i.e., in small micelles in the aqueous phase, in larger emulsion droplets of the organic phase, or in water outside of emulsions[11,12]).

Emulsion droplet size, physical environment, and composition under these conditions are highly challenging-to-impossible to study with traditional analytical techniques due to existing requirements for homogenous phase, high vacuum, or optical transparency (e.g., by NMR spectroscopy, transmission electron microscopy, or dynamic light scattering, respectively) (Figure 1). Understanding of these phase-separated systems therefore remains substantially limited to computational studies[13,14] and/or information derived from the isolation or study of reaction components under nonsynthetic conditions (e.g., under high vacuum, without organic substrate, and/or at much lower surfactant and/or substrate concentrations where phase separation does not occur).[10,15–17]

Yet, the behavior and changing compositions of the organic emulsion droplets over the course of a reaction-in-progress are of keen interest due to their high local concentrations of organics and subsequent anticipated impact on reaction rate, selectivity, and yield. We recently developed the spatial resolution and microenvironmental sensitivity of fluorescence lifetime imaging microscopy (FLIM)[18–20] to provide missing information on the size of emulsion droplets and the partitioning of select reagents under conditions relevant to synthesis, making it an emerging analytical technique in this area.[21–23] Specifically, FLIM is the creation of (spatially resolved) images that display the amount of time fluorescent molecules spend in their excited states.

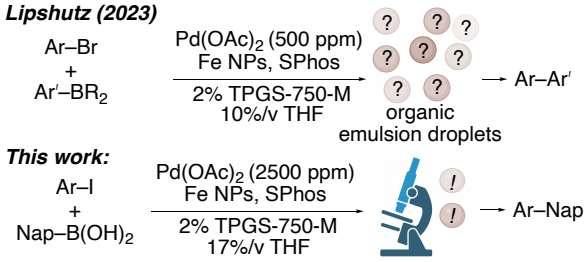

Figure 1. Reaction schematic of previous work, showing unknown emulsion behavior; reaction characterized herein.

To date, evolution of a full catalytic reaction from substrate-to-product in organic–aqueous–surfactant media has not been imaged by FLIM, or by any other type of microscopy, leading to several central questions: 1) *Do generated species build up during the reaction, and if so in which location(s)?* 2) *Does the buildup correlate (or anticorrelate) with bench-scale synthetic yields?* 3) *Is there environmental heterogeneity among emulsion droplets during an ongoing reaction?* 4) *To what extent does active catalyst generation (or lack thereof) impact reaction rate or underpin the need for organic cosolvents*?

https://doi.org/10.26434/chemrxiv-2024-jt42x **ORCID:** https://orcid.org/0000-0002-8055-1405

Palladium remains the most effective catalyst for many cross-coupling reactions such as the Suzuki reaction, but its cost and toxicity[24] have led to considerable effort to reduce the overall quantity required.[1,7,24–30] Lipshutz developed a synergistic iron nanoparticle (Fe-NP) based coupling reaction to reduce the palladium loading to as little as 500–2500 ppm.[1,7,25–27,31] This general system was chosen for study by FLIM. Specifically, the fluorescence lifetimes of organic fluorophores are exquisitely sensitive to their microenvironments.[18–23] We envisioned that a hydrophobic spectator fluorophore, **1**, doped in at the low loading of 220 nM, would inform on changes in composition of emulsion droplets though changes in its fluorescence lifetime, without chemical involvement in the reaction itself.[21,22,32,33] The anticipated changes in fluorescence lifetime **1** with reaction progress are not known in advance and therefore form part of the research question and technique development process.[32,34]

Results and Discussion

As shown in Figure 1, a cross-coupling reaction with TPGS-750-M surfactant was examined, with 4-iodoanisole (**2**), 1-naphthalene-boronic acid (**3**), $Pd(OAc)_2$, K_3PO_4, SPhos, and Fe NPs, using similar substrates, concentrations, and catalysts to the successful literature cross-coupling reaction.[25] The reaction proceeded at 45 °C. To generate high yields, a fast reaction rate, and enhanced reproducibility in our hands, the palladium loading was increased to 0.25 mol % (from 0.05 mol %) an alkyl iodide was selected over an alkyl bromide, and the THF cosolvent was increased to 17% v/v. Many reagents were only sparingly soluble in the surfactant solution, creating a thick, optically opaque slurry, as has been previously well-documented (including with published images) for such aqueous–organic–surfactant systems.[10] Due to the heterogeneous nature of the phase-separated reactions, two or more replicate experiments were performed per reaction condition for all data acquisition (see SI for images of replicate runs).

Imaging agent **1** contained a boron dipyrromethene core (BODIPY), which was selected for its high quantum yield, chemical inertness, small size relative to the emulsions and nanoparticles, and hydrophobicity[21,22,32,34–38] (Figure 2a). Imaging agent **1** was added as a spectator fluorophore at a low concentration (220 nM) to enable imaging and sensing of environmental changes through changes in its fluorescence lifetime. For comparison, the concentrations of other components were 0.6 M boronic acid **3**, 0.5 M 4-iodoanisole **2**, 1.1 mM palladium acetate, 25 mM SPhos, 5 mol % Fe NP, 2 wt % TPGS-750-M. Thus, the organic substrates were over 6 orders of magnitude higher in concentration than **1**. At this low doping, the imaging agent is unlikely to significantly perturb partitioning of the system. Images were obtained ~1 µm above the bottom of the imaging vial. Complementary brightfield images were also taken.

With the goal of assessing FLIM's ability to provide interpretable images in this system, an initial emulsion system was examined. FLIM images from 2.5 h after initiation, shown in Figure 2b, are false-colored on a rainbow scale to display spatial differences in fluorescence lifetime ($\tau_{ave\ int}$), reflecting differentiation of local microenvironments. Blue-shifted regions represent shorter fluorescence lifetimes, and red-shifted regions represent longer fluorescence lifetimes.

Comparison of FLIM and brightfield images of the same region establish that emulsion droplets and NP–surfactant rafts[1] can be generally identified by differences in opacity, shape, brightness, and $\tau_{ave\ int}$ (Figure 2b). Nanoparticle rafts were somewhat opaque, irregularly shaped, exhibited dim fluorescence, and on average had lower $\tau_{ave\ int}$. Emulsion droplets were optically transparent, generally spherical, exhibited brighter fluorescence, and on average had higher $\tau_{ave\ int}$. The focal plane for FLIM is narrow (~600 nm), leading to a researcher-selected, narrow cross section in z in each acquired image. In contrast, brightfield has a substantially deeper focal plane. Thus, substantially more materials are visible in the brightfield image than in the FLIM image because the materials are at different depths in the sample and thus lie outside of FLIM's narrow focal plane.

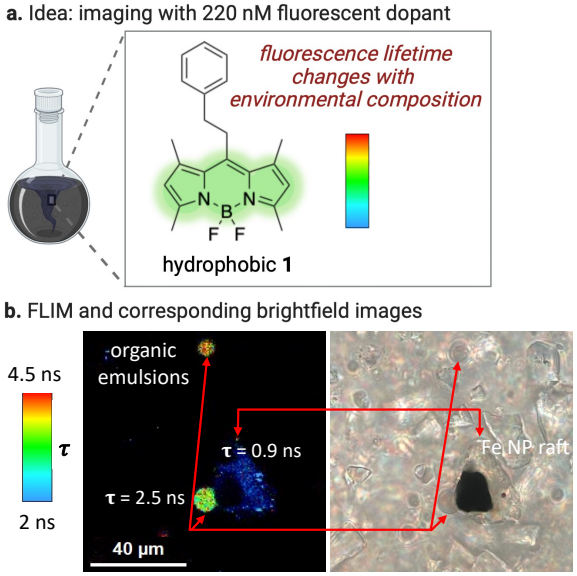

Figure 2. (a) Schematic overview of FLIM idea to image reaction behavior with spectator imaging agent **1**. **(b)** Fe NP rafts and emulsion droplets imaged by FLIM and corresponding brightfield microscopy.

Because chemical reactions intrinsically cause changes in concentrations as starting materials are consumed, products are formed, catalysts dissolve and decompose, and reaction intermediates may build up, the concentration-dependent impact on $\tau_{ave\ int}$ of **1** of each (known) reaction component was next measured through a series of solution-phase analyses. The outcomes of these individual analyses are summarized in Table 1 (full data in SI). Specifically, all measured components that had an effect on lifetime, had the effect of quenching fluorescence, resulting in shorter fluorescence lifetimes (reduction in $\tau_{ave\ int}$ of **1**, see SI for fluorescence quenching data)[19] or having no effect on lifetime. Notably, no components increased lifetime. The concentration-dependent lifetime change in ns/mM was determined from the linear regression of the concentration-dependent lifetime calibration curve (column 1).

The concentration of each reaction component at $t = 0$ for cross-coupling and imaging conditions was known, on the basis of what was added to the reaction mixtures (column 2). Multiplication of column 1 by column 2 enabled estimation of the impact in ns of each component on $\tau_{ave\ int}$ of **1** at the start of the reaction under early reaction conditions. A limitation of this estimation is that values in Table 1 were intentionally derived from simplified systems containing only solvent (THF or 2 wt % TPGS-750-M), **1**, and the component of interest. For most

entries, these conditions produced homogeneous solutions. In contrast, under reaction conditions, the high concentrations of organic substrates induced phase separation with formation of large emulsion droplets.

As deduced from Table 1, the components indicated to have the strongest overall quenching effect on imaging agent **1** at the concentrations of the initial reaction are Fe NPs (insoluble; suspended in THF), SPhos, and **2**, and the combination of $Pd(OAc)_2$ with SPhos (column 3). The large impact of palladium-derived species on $\tau_{ave\ int}$ was envisioned to be helpful for characterizing catalyst location and evolution.

Table 1. Measured and Anticipated Lifetime Effects of Reaction Components on Imaging Agent **1**.

Reagent	concentration-dependent lifetime change (ns/mM)	concentration in reaction (mM)	anticipated lifetime effect under reaction conditions (ns)
in micelles/ in droplets			
Fe NPs	−0.0045	120	−0.5
SPhos	−0.015	25	−0.4
4-iodoanisole	−0.0007	500	−0.4
$Pd(OAc)_2$ + SPhos	−0.25	1.2[a]	−0.3
$Pd(OAc)_2$	−0.15	1.2	−0.2
1-(4-methoxyphenyl)-naphthalene	−0.0002	500[b]	−0.1
1-naphthalene boronic acid	−0.00008	600	n.a.[c]
commercial Pd NPs	0.0054	1.2	n.a.[c]
in aqueous			
K_3PO_4	− 0.0025	1000	−2.5
HK_2PO_4	−0.0013	1000[d]	−1.3

[a] by Pd concentration. [b] if reaction goes to completion, concentration of product would be 500 mM. [c] anticipated effect is below the detection limit of the instrument. [d] if all the K_3PO_4 protonates, the concentration would be 1000 mM.

In contrast, the boronic acid and an authentic sample of the cross-coupling product 1-(4-methoxyphenyl)-naphthalene (**4**) did not show an appreciable impact on $\tau_{ave\ int}$ over the relevant concentration range.

To determine if the potential formation of palladium black through catalyst decomposition during the reaction would have an appreciable effect on lifetime, the impact of commercial Pd(0) NPs on the fluorescence lifetime of **1** was investigated. Specifically, commercial Pd(0) NPs were suspended in aqueous–surfactant solution (see Supporting Information for additional measurements of Pd(0) NPs in THF). No effect on the lifetime of **1** occurred. Thus, within the limitations of commercial NPs to accurately resemble heterogeneous catalyst decomposition, palladium black was unlikely to affect the FLIM measurement during the forthcoming FLIM experiments.

While the ionic and highly water-soluble phosphates strongly affected the lifetime of **1** in the calibration measurements in Table 1, these salts and hydrophobic **1** are unlikely to be in the same phase after organic substrates are added and phase separation occurs.[11,13,39] Thus, during reaction imaging, phosphates and are unlikely to appreciably impact the lifetime of **1** within the emulsion droplets.

With a baseline understanding of the impact of individual components on the fluorescence lifetime readout of the reporter, **1**, the chemical evolution of the full cross-coupling reaction system was investigated. First, the reaction was performed with an order of addition analogous to that reported by Lipshutz., $Pd(OAc)_2$ was added last to the reaction mixture, in THF (Figure 3a). This addition was the source of all the THF, bringing the total to 17 wt/%. The time of addition of the $Pd(OAc)_2$ in THF was defined as $t = 0$ min. For clarity, we will call this order of addition the "non-premixed catalyst". The reaction was initiated at 45 °C. For imaging, aliquots of the reaction slurry were removed from a vigorously stirring reaction vessel and transferred to a nitrogen-purged microscopy vial at timepoints and imaged using time-resolved confocal fluorescence microscopy. Obtaining images from two timepoints prior to addition of catalyst enabled documentation of the effect of the initial mixing to distribute substrates into the droplets.

Representative FLIM images of system evolution with reaction progress are shown in Figure 3a. Additional images are available in the SI. Values of $\tau_{ave\ int}$ correspond to emulsion droplets specifically, which were selected and evaluated as regions of interest (ROIs). Values are derived from averages of $n \geq 30$ droplets from two or more replicate runs and multiple imaging regions from each run. Imaging data show the following key features:

1) Emulsion droplets were visible at all timepoints.

2) Emulsion droplet sizes ranged from ~2 μm to ~50 μm.

3) Prior to catalyst addition, initial $\tau_{ave\ int}$ decreased rapidly, as stirring distributed substrates into droplets.

4) Upon addition of palladium acetate in THF immediately after acquisition of the $t = 0$ images, $\tau_{ave\ int}$ remained relatively similar throughout the chemical reaction progress.

a. non-premixed palladium

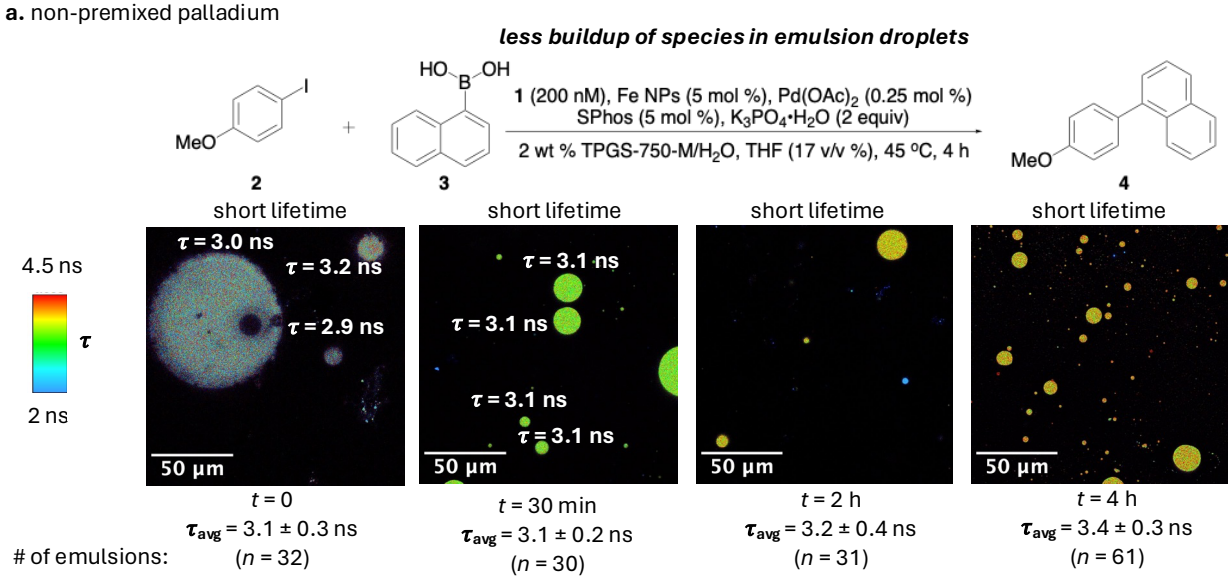

b. premixed palladium

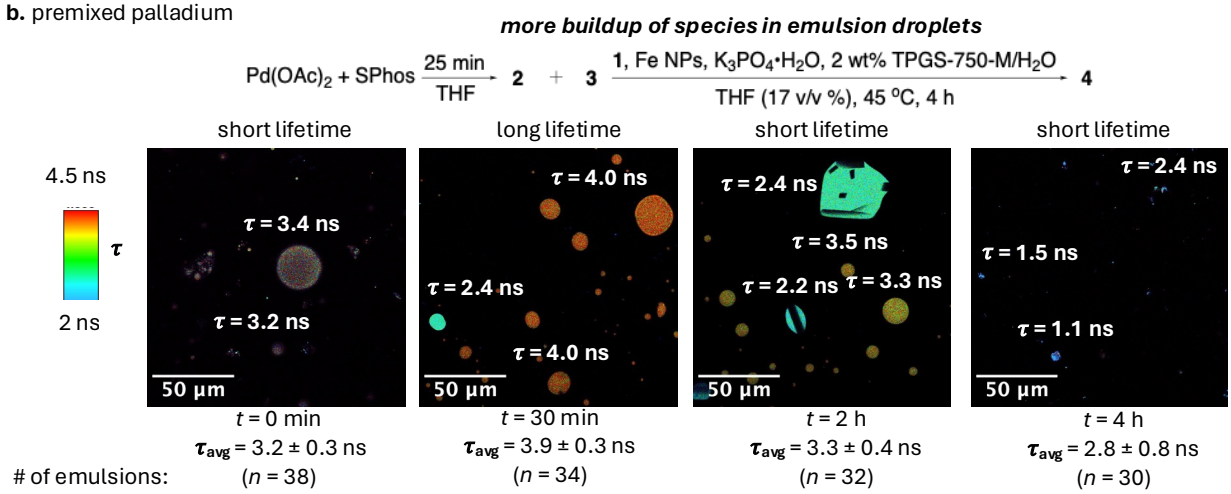

c. lifetime vs. reaction progress of reactions

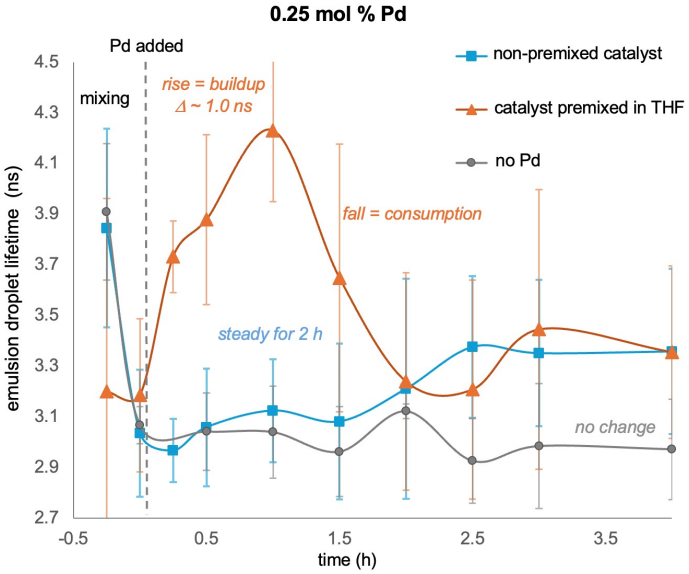

d. isolated yields under different conditions

conditions	yield 1 h (%)	yield 2 h (%)
non-premixed Pd	29 ± 6	95 ± 0
premixed Pd + SPhos	90 ± 5	83 ± 3
no THF	13 ± 11	47 ± 15

Figure 3. (a) Emulsion droplets show little change under standard reaction conditions. **(b)** The reaction with the premixed catalyst: emulsion droplets show evidence for rapid species buildup and consumption. **(c)** Fluorescence lifetime vs. reaction progress of the reactions. **(d)** Isolated yields under different conditions with 0.25 mol % palladium.

5) Intrinsic environmental heterogeneities among emulsion droplets are reflected in emulsion droplets of different false colors, and the degree of heterogeneity among droplets is estimated by the standard deviation among droplet fluorescent lifetimes.

6) The average size of emulsion droplets decreased slightly with reaction progress, presumably from the consumption of starting materials, which decreased the suspended organics. (The cross-coupling product formed a largely insoluble solid clump as the reaction progressed.)

Figure 3c graphically presents the $\tau_{ave\ int}$ data with time, derived from the suite of experiments that produced the representative images in Figure 3a (blue data). The lines are guides for the eye and are not mathematical fits. A control experiment in which palladium was not added, but rather only the same quantity of blank THF was added at $t = 0$, appears similar, exhibiting constant $\tau_{ave\ int}$ with time (gray data). Thus, no FLIM outcomes from the imaging data in Figure 3a during the critical first 2 h of the reaction were assigned to the behaviors of palladium or to detectable changes in compositions of emulsion droplets from the cross-coupling reaction, despite the confirmed consumption of starting materials and generation of product on the bench-scale under these conditions, as next described.

The table in Figure 3d shows bench-scale isolated reaction yields from parallel experiments run under identical conditions to the microscopy imaging experiments, at $t = 1$ h (29% ± 6) and 2 h (95% ± 0). The lower yield at 1 h than at 2 h demonstrates that the reaction with non-premixed catalyst displays an induction period. Brightfield images clearly identify substantial insoluble SPhos in these solvent systems (Figure 4); thus, the induction period is assigned to slow formation of the active catalyst due to insoluble precatalyst components. The "slow start" of the reaction was hypothesized to contribute to the absence of detectible changes to the compositions of the emulsion droplets, i.e., any reaction intermediates were building up too slowly to detect by their impact on the droplet environment.

In contrast, a comparison reaction system that deviated from published synthetic procedure with a predissolved/premixed catalyst, where $Pd(OAc)_2$ and SPhos were predissolved in THF for ~25 min prior to addition to the reaction, resulted in dramatic and rapid changes in in droplet composition, as seen by a dramatic increase in $\tau_{ave\ int}$ (Figure 3b). (SPhos readily dissolved in THF but was largely insoluble in TPGS–water.) The same total quantity of THF (along with the premixed catalyst) was added at $t = 0$ as THF that had been added at $t = 0$ in the non-premixed catalyst runs. The lifetimes inside the emulsion droplets dramatically increased (as seen by the redshift), then decreased at $t = 2$ h (blueshift), consistent with buildup and consumption of species.

This fast buildup and consumption correlated with a faster bench-scale reaction. The premixed condition result in high isolated yields at both 1 h (90 ± 5%) and 2 h (83 ± 3%), indicating that product formation is essentially complete within the first hour (Figure 3d). (The two yields are within standard deviations from replicates, such that yields are not interpretated as decreasing after 1 h.) Thus, premixing the palladium and ligand in THF increased the early rate of the reaction, likely by bypassing SPhos solubility restrictions.[40–45]

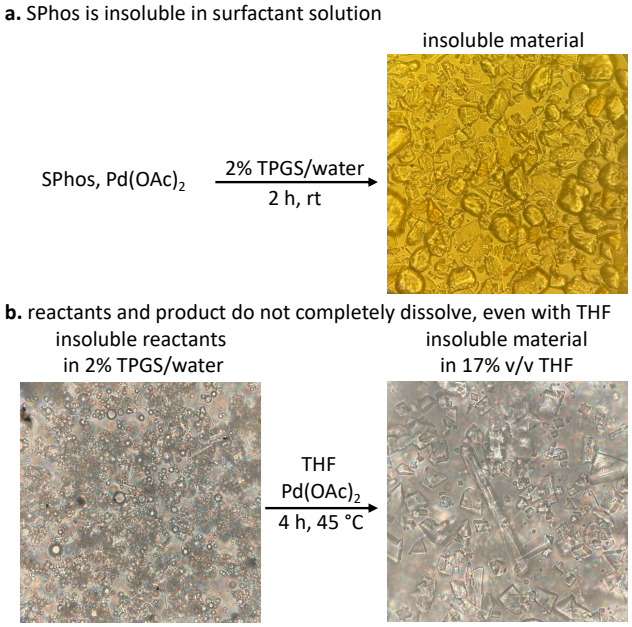

Figure 4. Brightfield images establish: **(a)** SPhos does not substantially dissolve in TPGS–water solution, even with $Pd(OAc)_2$ and vigorous stirring for 2 h. **(b)** A full reaction system with 4-iodoanisole, boronic acid, SPhos, and potassium phosphate in 2% TPGS–water, followed by the addition of $Pd(OAc)_2$ and 17 v/v % THF, has substantial insoluble material present over the full course of the reaction.

Importantly, the addition of the premixed palladium catalyst, on its own, without reaction with the substrates, would have been expected to lower lifetime, not raise it (see Table 1), the opposite of the observed effect. Similarly, if the long lifetimes were simply caused by consumption of the quenching iodoanisole substrate, then the lifetime would increase and then stabilize at a consistent, high value; however, lifetime increases and then decreases, consistent with buildup of a species followed by its consumption.

Because no known reaction component *raises* the lifetime of **1**, the initial interpretation of these data centers on scenarios in which quenching components decrease in concentration with time, replaced by components with less-or-no quenching, resulting in higher droplet fluorescence lifetimes. The alterative—that is, the presence of yet-unidentified chemical species leading to higher fluorescence lifetimes[32]—remains possible.

Although the structure(s) of the species inside the emulsion droplets during the readout of high lifetimes remain unknown, one possibility is that this effect is caused by the kinetic buildup of cross-coupling product **4**. Thus, FLIM captures a persistent, intermediate kinetic state, during which droplets are swollen with product **4** before **4** precipitates. Because **4** does not quench **1** (Table 1), the overall concentration of quenching agents is reduced (through dilution) inside the droplets during this reaction stage, resulting in higher fluorescence lifetimes. Subsequent precipitation of **4** then results in its consumption from the droplets, with accompanying reduction in droplet fluorescence lifetime. Consistent with this interpretation, droplets become smaller and display low fluorescence lifetimes at 4 h, a duration after that needed for complete conversion (Figure 3b).

An alternative possibility is that the species inside the droplets at this stage are chemical intermediates; for example,

organopalladium or other post-oxidative addition or post-transmetalation intermediates. The quenching iodide equivalent or $B(OH)_3$ equivalent thus has been shunted outside the droplet, into the aqueous phase as $IB(OH)_3^-$ or related inorganic complexes.[46] Additional chemical possibilities cannot currently be ruled out.

The evolution of a reaction system at 10× catalyst loading was examined next, with 2.5 mol % palladium, rather than with 0.25 mol % palladium (Figure 5, green data). In this case, similar FLIM trends of rise-and-fall (assigned to buildup-and-consumption) occurred but on a much faster timescale. This observation is consistent with a faster droplet composition change occurring as a consequence of higher catalyst loading, and thus supports the premise that the changes in droplet composition are *caused* by catalysis.

Next, the types of reaction(s) capable of leading to increases in fluorescence lifetimes were pinpointed to specific substrates through exclusion experiments. Emulsion droplets were observed in both exclusion samples despite the absence of one of the two substrates, enabling similar ROI analysis (see SI for images). Because the starting composition of the droplets were different in these exclusion experiments, the *change* in fluorescence lifetime, $\Delta\tau_{ave\ int}$, with reaction progress, rather than absolute $\tau_{ave\ int}$ was evaluated.

The 4-iodoanisole was first omitted, such that the boronic acid was the only substrate at $t = 0$ (Figure 5, purple data). After 2.5 mol % catalyst addition, droplet fluorescence lifetime rose rapidly and markedly ($\Delta\tau \sim 1.5$ ns). This marked rise suggests a similar process may be occurring in the absence of 4-iodoanisole, i.e., that oxidative addition is not required for the environmental change that is assigned to species buildup. One possibility for a palladium-catalyzed reaction of boronic acid alone is boronic acid homocoupling.[47] Although, the catalytic turnover required to produce this outcome is less likely here given the air-free conditions that deprive the system of a known stochiometric oxidant. A second possibility is that the addition of the THF that accompanies catalyst addition promotes a repartitioning of the boronic acid into the aqueous phase as it forms anionic boronate complexes;[46] however, that hypothesis was ruled out because it does not involve the action of palladium. Therefore, it is inconsistent with the observed absence of change without catalyst when the same amount of THF was added alone (Figure 3c, gray data). The presence of an unknown stoichiometric oxidant or of a catalytic cause of repartitioning would be therefore required for the action these two hypotheses, respectively.

Next, boronic acid **3** was omitted, such that iodoanisole **2** was the only substrate at $t = 0$. The fluorescence lifetime of the emulsion droplets remained relatively consistent over 1.5 h. Importantly, a substantial rise beyond droplet range and measurement variability does not occur. Thus, **2** alone or buildup of an oxidative addition organopalladium intermediate alone do not appear capable of causing the detected environmental changes assigned to buildup and consumption. The conclusion of these substrate-exclusion experiments is that the full reaction sequence or the reactions of the boronic acid with catalyst are those capable of producing increases in fluorescence lifetimes. This information is helpful at ruling out possibilities for species in the droplets causing high lifetimes (e.g., those from oxidative addition alone), but it is insufficient for clearly differentiating among the full suite of the hypotheses described above.

In order to further examine the plausibility of rate-limiting catalyst solubilization, the role of the THF cosolvent in this system was closely examined. In many optimized aqueous–organic surfactant reactions, an organic cosolvent is added.[16,48] A predominant mechanistic rationale for the favorable effect of the cosolvent is that it increases the size of the micellar interior.[10,13,26] Alternative proposals include that the cosolvent assists with solubilization to distribute reagents and catalyst within the micelles; maintains vapor pressure of volatile reagents; and prevents buildup on magnetic stir bars[10,49].

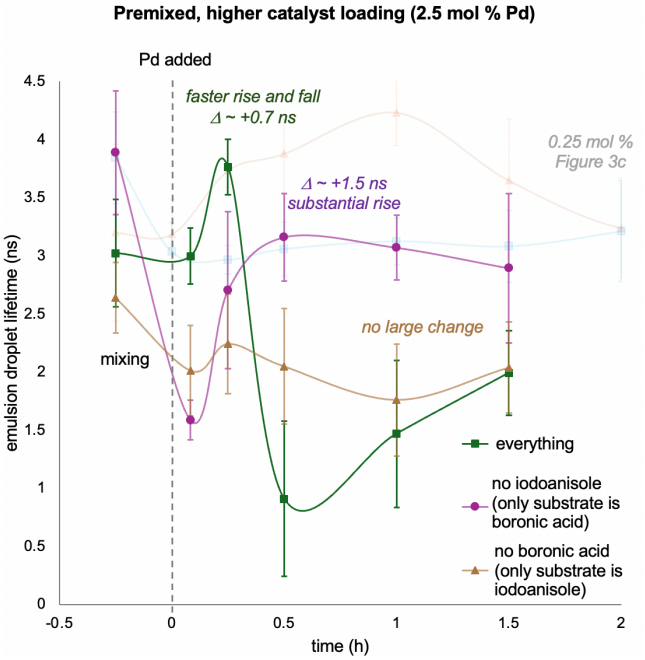

Figure 5. Lifetime vs. reaction progress of the reactions with 2.5 mol % Pd loading, including comparison with substrate exclusion experiments.

To examine these possibilities, synthesis in the absence of THF was performed. In the absence of THF, individual microscopy reaction runs were substantially more variable. For example, in one run, the emulsion droplets were visible at $t = 15$ min, but in another were not visible until $t \sim 2$ h. (See SI for full images and comparisons of triplicate runs.) This variability at the microscale tracked with variability on the macroscale of isolated yields of **4**, as seen by higher standard deviations in the table in Figure 3d. Further, yields were substantially lower. Together, these data support a model where the overall rate and variability of the cross-coupling reaction is heavily dependent on solubilization by THF of the poorly soluble catalyst precursors, a step required to precede formation of the active catalyst. Premixing the catalyst components in THF prior to addition to the aqueous medium overcomes this time-dependent solubility and its associated batch-to-batch variability.

Conclusion

The questions posed at the beginning of the study have been answered. Data is consistent with: 1) Generated species build up in the emulsion droplets, when there is a higher effective loading of catalyst. This higher loading occurs when either

the components are added in a greater quantity (e.g., 2.5 mol % rather than 0.25 mol %), or when generating the active catalyst in advance by predissolving the catalyst components. 2) Faster buildup and consumption inside the droplets correlates with faster bench-scale reaction rate; 3) Droplet heterogeneity over the course of the reaction is evident and characterizable by droplet-to-droplet FLIM differences; and, 4) A key role of the THF cosolvent is solubilization of otherwise solid precatalyst components to generate the active catalyst(s), without which, changes in emulsion droplet composition are stalled, along with stalling of accompanying product formation.

This combination of microscale (FLIM) imaging and macroscale (isolated reaction yield) data identified a correlation between the buildup and consumption of species inside the emulsion droplets and bench-scale cross-coupling reaction rates. Though the exact structure(s) of these species remain unknown, their impact on FLIM signals during the ongoing reaction nevertheless provided an actionable model for reaction improvement by providing a successful strategy to bypass the induction period through predissolving the catalyst. More broadly, spatially resolved imaging with FLIM shed light on the how the bench-scale reaction progress correlates with changes in emulsion droplet compositions, a previously intractable experimental measurement.

ASSOCIATED CONTENT

Supporting Information

The Supporting Information is available free of charge

Detailed experimental procedures and replicate fluorescence lifetime imaging microscopy data (PDF)

AUTHOR INFORMATION

Corresponding Author

* Suzanne A. Blum − *Department of Chemistry, University of California, Irvine, Irvine, California 92697-2025, United States;* orcid.org/0000-0002-8055-1405;
Email: blums@uci.edu

Author

Hannah Peacock − *Department of Chemistry, University of California, Irvine, Irvine, California 92697-2025, United States;* orcid.org/0000-0002-8967-2027

Notes

The authors declare no competing financial interest.

ACKNOWLEDGMENT

The authors thank the National Institute of Health (R01GM131147), the Allergan Foundation for a fellowship to HP, and the University of California, Irvine, for funding, and Professor Bruce Lipshutz, Dr. Yuting Hu, and Karthik Iyer (UCSB) for nanoparticles, surfactant, and helpful discussions. We thank Alexis C. Ravenscroft for assistance obtaining concentration-dependent lifetime data and early optimization. Figures were created with BioRender.

REFERENCES

(1) Handa, S.; Wang, Y.; Gallou, F.; Lipshutz, B. H. "Sustainable Fe-ppm Pd nanoparticle catalysis of Suzuki-Miyaura cross-couplings in water." *Science* **2015**, *349*, 1087–1091.

(2) La Sorella, G.; Strukul, G.; Scarso, A. "Recent advances in catalysis in micellar media." *Green Chem.* **2015**, *17*, 644–683.

(3) Lipshutz, B. H.; Taft, B. R.; Abela, A. R. "Catalysis in the Service of Green Chemistry: Nobel Prize-Winning Palladium-Catalysed Cross-Couplings, Run in Water at Room Temperature." *Platin. Met. Rev.* **2012**, *56*, 62–74.

(4) Gallou, F.; Isley, N. A.; Ganic, A.; Onken, U.; Parmentier, M. "Surfactant technology applied toward an active pharmaceutical ingredient: more than a simple green chemistry advance." *Green Chem.* **2015**, *18*, 14–19.

(5) J. Fox, R.; Daniel Bailey, J.; Victoriano Obligacion, J.; Borlinghaus, N.; M. Braje, W.; Li, X.; Mukherjee, S.; Schoen, A.; B. Towne, T.; Vukelić, S. "Chemistry in Water Reproducibility Study: Learnings from a Precompetitive, Multicompany Collaboration." *Org. Process Res. & Dev.* **2024**, *0*.

(6) Petkova, D.; Borlinghaus, N.; Sharma, S.; Kaschel, J.; Lindner, T.; Klee, J.; Jolit, A.; Haller, V.; Heitz, S.; Britze, K.; Dietrich, J.; Braje, W. M.; Handa, S. "Hydrophobic Pockets of HPMC Enable Extremely Short Reaction Times in Water." *ACS Sustain. Chem. Eng.* **2020**, *8*, 12612–12617.

(7) Hu, Y.; Wong, M. J.; Lipshutz, B. H. "ppm Pd-Containing Nanoparticles as Catalysts for Negishi Couplings … in Water." *Angew. Chem., Int. Ed.* **2022**, *61*, e202209784.

(8) Takale, B. S.; Thakore, R. R.; Irvine, N. M.; Schuitman, A. D.; Li, X.; Lipshutz, B. H. "Sustainable and Cost-Effective Suzuki-Miyaura Couplings toward the Key Biaryl Subunits of Arylex and Rinskor Active." *Org. Lett.* **2020**, *22*, 4823–4827.

(9) Sharma, S.; Buchbinder, N. W.; Braje, W. M.; Handa, S. "Fast Amide Couplings in Water: Extraction, Column Chromatography, and Crystallization Not Required." *Org. Lett.* **2020**, *22*, 5737–5740.

(10) Gabriel, C. M.; Lee, N. R.; Bigorne, F.; Klumphu, P.; Parmentier, M.; Gallou, F.; Lipshutz, B. H. "Effects of co-solvents on reactions run under micellar catalysis conditions." *Org. Lett.* **2017**, *19*, 194–197.

(11) Boyer, B.; Hambardzoumian, A.; Roque, J. P.; Beylerian, N. "Inverse phase transfer catalysis versus interfacial catalysis. Effect of medium stirring in the epoxidation reaction of chalcone by hydrogen peroxide." *J. Chem. Soc. Perkin Trans. 2* **2002**, *2*, 1689–1691.

(12) Hauk, P.; Wencel-Delord, J.; Ackermann, L.; Walde, P.; Gallou, F. "Organic synthesis in Aqueous Multiphase Systems — Challenges and opportunities ahead of us." *Curr. Opin. Colloid Interface Sci.* **2021**, *56*, 101506.

(13) Andersson, M. P.; Gallou, F.; Klumphu, P.; Takale, B. S.; Lipshutz, B. H. "Structure of Nanoparticles Derived

from Designer Surfactant TPGS-750-M in Water, As Used in Organic Synthesis." *Chem. Eur. J.* **2018**, *24*, 6778–6786.

(14) Ranaudo, A.; Greco, C.; Moro, G.; Zucchi, A.; Mattiello, S.; Beverina, L.; Cosentino, U. "Partition of the Reactive Species of the Suzuki–Miyaura Reaction between Aqueous and Micellar Environments." *J. Phys. Chem. B* **2022**, *126*, 9408–9416.

(15) Molyneux, S.; J. M. Goss, R. "Fully Aqueous and Air-Compatible Cross-Coupling of Primary Alkyl Halides with Aryl Boronic Species: A Possible and Facile Method." *ACS Catal.* **2023**, *13*, 6365–6374.

(16) Sherwood, J.; Clark, J. H.; Fairlamb, I. J. S.; Slattery, J. M. "Solvent effects in palladium catalysed cross-coupling reactions." *Green Chem.* **2019**, *21*, 2164–2213.

(17) Zuo, Y.-J.; Qu, J. "How Does Aqueous Solubility of Organic Reactant Affect a Water-Promoted Reaction?" *J. Org. Chem.* **2014**, *79*, 6832–6839.

(18) Berezin, M. Y.; Achilefu, S. "Fluorescence Lifetime Measurements and Biological Imaging." *Chem. Rev.* **2010**, *110*, 2641–2684.

(19) van Munster, E. B.; Gadella, T. W. J. In *Microscopy Techniques*; Rietdorf, J., Ed.; Springer Berlin Heidelberg: Berlin, Heidelberg, 2005; pp 143–175.

(20) Datta, R.; Heaster, T. M.; Sharick, J. T.; Gillette, A. A.; Skala, M. C. "Fluorescence lifetime imaging microscopy: fundamentals and advances in instrumentation, analysis, and applications." *J. Biomed. Opt.* **2020**, *25*, 07123.

(21) Peacock, H.; Blum, S. A. "Single-Micelle and Single-Zinc-Particle Imaging Provides Insights into the Physical Processes Underpinning Organozinc Reactions in Water." *J. Am. Chem. Soc.* **2022**, *144*, 3285–3296.

(22) Peacock, H.; Blum, S. A. "Surfactant Micellar and Vesicle Microenvironments and Structures under Synthetic Organic Conditions." *J. Am. Chem. Soc.* **2023**, *145*, 7648–7658.

(23) Zhang, Y.; Blum, S. A. "Surfactant-Dependent Partitioning of Organics in Aqueous – Organic Reaction Systems." *ChemRxiv* **2024**, doi:10.26434/chemrxiv-2024-zjhtg.

(24) Farina, V. "High-turnover palladium catalysts in cross-coupling and Heck chemistry: A critical overview." *Adv. Synth. Catal.* **2004**, *346*, 1553–1582.

(25) Hu, Y.; Li, X.; Jin, G.; Lipshutz, B. H. "Simplified Preparation of ppm Pd-Containing Nanoparticles as Catalysts for Chemistry in Water." *ACS Catal.* **2023**, *13*, 3179–3186.

(26) Pang, H.; Hu, Y.; Yu, J.; Gallou, F.; Lipshutz, B. H. "Water-Sculpting of a Heterogeneous Nanoparticle Precatalyst for Mizoroki-Heck Couplings under Aqueous Micellar Catalysis Conditions." *J. Am. Chem. Soc.* **2021**, *143*, 3373–3382.

(27) Handa, S.; Jin, B.; Bora, P. P.; Wang, Y.; Zhang, X.; Gallou, F.; Reilly, J.; Lipshutz, B. H. "Sonogashira Couplings Catalyzed by Fe Nanoparticles Containing ppm Levels of Reusable Pd, under Mild Aqueous Micellar Conditions." *ACS Catal.* **2019**, *9*, 2423–2431.

(28) Thakore, R. R.; Takale, B. S.; Gallou, F.; Reilly, J.; Lipshutz, B. H. "N, C-Disubstituted Biarylpalladacycles as Precatalysts for ppm Pd-Catalyzed Cross Couplings in Water under Mild Conditions." *ACS Catal.* **2019**, *9*, 11647–11657.

(29) Roy, D.; Uozumi, Y. "Recent Advances in Palladium-Catalyzed Cross-Coupling Reactions at ppm to ppb Molar Catalyst Loadings." *Adv. Synth. Catal.* **2018**, *360*, 602–625.

(30) Ram, S.; Mehara, P.; Kumar, A.; Sharma, A. K.; Chauhan, A. S.; Kumar, A.; Das, P. "Supported-Pd catalyzed carbonylative synthesis of phthalimides and isoindolinones using Oxalic acid as in situ CO surrogate with 2-iodobenzamides and 2-iodobenzylanilines in ppm-level catalyst loading." *Mol. Catal.* **2022**, *530*, 112606.

(31) Wu, B.; Miraghaee, S.; Handa, S.; Gallou, F. "Nanoparticles for catalysis in aqueous media." *Curr. Opin. Green Sustain. Chem.* **2022**, *38*, 100691.

(32) Garcia IV, A.; A. Blum, S. "Polymer Molecular Weight Determination via Fluorescence Lifetime." *J. Am. Chem. Soc.* **2022**, *144*, 22416–22420.

(33) Easter, Q. T.; A. Blum, S. "Organic and Organometallic Chemistry at the Single-Molecule, -Particle, and -Molecular-Catalyst-Turnover Level by Fluorescence Microscopy." *Acc. Chem. Res.* **2019**, *52*, 2244–2255.

(34) Hanada, E. M.; Tagawa, T. K. S.; Kawada, M.; Blum, S. A. "Reactivity Differences of Rieke Zinc Arise Primarily from Salts in the Supernatant, Not in the Solids." *J. Am. Chem. Soc.* **2022**, *144*, 12081–12091.

(35) Eivgi, O.; Blum, S. A. "Real-Time Polymer Viscosity-Catalytic Activity Relationships on the Microscale." *J. Am. Chem. Soc.* **2022**, *144*, 13574–13585.

(36) Easter, Q. T.; Blum, S. A. "Single Turnover at Molecular Polymerization Catalysts Reveals Spatiotemporally Resolved Reactions." *Angew. Chem., Int. Ed.* **2017**, *56*, 13772–13775.

(37) Hanada, E. M.; Jess, K.; Blum, S. A. "Mechanism of an Elusive Solvent Effect in Organozinc Reagent Synthesis." *Chem. Eur. J.* **2020**, *26*, 15094–15098.

(38) Jess, K.; Kitagawa, K.; Tagawa, T. K. S.; Blum, S. A. "Microscopy Reveals: Impact of Lithium Salts on Elementary Steps Predicts Organozinc Reagent Synthesis and Structure." *J. Am. Chem. Soc.* **2019**, *141*, 9879–9884.

(39) Ceriani, C.; Ghiglietti, E.; Sassi, M.; Mattiello, S.; Beverina, L. "Taming troublesome suzuki-miyaura reactions in water solution of surfactants by the use of lecithin: A step beyond the micellar model." *Org. Process Res. Dev.* **2020**, *24*, 2604–2610.

(40) Yoo, K. S.; Park, C. P.; Yoon, C. H.; Sakaguchi, S.; O'Neill, J.; Jung, K. W. "Asymmetric intermodular heck-type reaction of acyclic alkenes via oxidative palladium(II) catalysis." *Org. Lett.* **2007**, *9*, 3933–3935.

(41) Yoo, K. S.; Yoon, C. H.; Jung, K. W. "Oxidative palladium(II) catalysis: A highly efficient and

chemoselective cross-coupling method for carbon-carbon bond formation under base-free and nitrogenous-ligand conditions." *J. Am. Chem. Soc.* **2006**, *128*, 16384–16393.

(42) Wu, X.; Fors, B. P.; Buchwald, S. L. "A Single Phosphine Ligand Allows Palladium-Catalyzed Intermolecular C□O Bond Formation with Secondary and Primary Alcohols." *Angew. Chemie* **2011**, *123*, 10117–10121.

(43) Bruno, N. C.; Buchwald, S. L. "Synthesis and application of palladium precatalysts that accommodate extremely bulky Di-tert-butylphosphino biaryl ligands." *Org. Lett.* **2013**, *15*, 2876–2879.

(44) Edwards, G. A.; Trafford, M. A.; Hamilton, A. E.; Buxton, A. M.; Bardeaux, M. C.; Chalker, J. M. "Melamine and melamine-formaldehyde polymers as ligands for palladium and application to Suzuki-Miyaura cross-coupling reactions in sustainable solvents." *J. Org. Chem.* **2014**, *79*, 2094–2104.

(45) Panteleev, J.; Zhang, L.; Lautens, M. "Domino Rhodium-Catalyzed Alkyne Arylation/Palladium-Catalyzed N Arylation: A Mechanistic Investigation." *Angew. Chemie* **2011**, *123*, 9255–9258.

(46) Lennox, A. J. J.; Lloyd-Jones, G. C. "Transmetalation in the Suzuki-Miyaura coupling: The fork in the trail." *Angew. Chem., Int. Ed.* **2013**, *52*, 7362–7370.

(47) Adamo, C.; Amatore, C.; Ciofini, I.; Jutand, A.; Lakmini, H. "Mechanism of the Palladium-Catalyzed Homocoupling of Arylboronic Acids: Key Involvement of a Palladium Peroxo Complex." *J. Am. Chem. Soc.* **2006**, *128*, 6829–6836.

(48) Shen, T.; Zhou, S.; Ruan, J.; Chen, X.; Liu, X.; Ge, X.; Qian, C. "Recent Advances on Micellar Catalysis in Water." *Adv. Colloid Interface Sci.* **2021**, *287*, 102299.

(49) Virdi, J. K.; Dusunge, A.; Handa, S. *JACS Au*. American Chemical Society January 16, 2023, pp 301–317.

Insert Table of Contents artwork here